Explicit Design of Geogrids with a Nonlinear Interface Model

F. Jacobs & M. Ziegler
Geotechnical Engineering, RWTH Aachen University, Germany

L. Vollmert
BBG Bauberatung Geokunststoffe GmbH & Co. KG, Espelkamp-Fiestel, Germany

H. Ehrenberg
NAUE GmbH & Co. KG, Espelkamp-Fiestel, Germany

ABSTRACT: An interaction model between geogrid and soil is being developed explicitly taking into account frictional and bearing resistance of geogrids during pull-out. The results of normal-sized pull-out tests at RWTH Aachen University are being used to evaluate the necessary input functions for the model, which is then validated with large pull-out tests. Additionally, field measurement data of an in-situ pull-out situation in a geogrid anchorage trench above a steep slope are presented that can be used for further validation. The results show that the developed model is capable of predicting the pull-out displacement and deformation of a geogrid as well as the geogrid force and junction loads at all positions along its anchorage length for any given load.

Keywords: Geogrid reinforced soil, pull-out, anchorage, nonlinear interaction model, mobilization

1 INTRODUCTION

All geogrid reinforced structures can be designed safely using limit state analysis. However, numerous field studies show that the actual load bearing capacities of geogrid reinforced structures are often much higher than the expected loads from calculations. This is caused by mostly still conservative design concepts that are based on empirical investigations, which cannot represent the real, deformation-dependent mechanical behavior of geogrid reinforced soil.

Regarding the pull-out situation of geogrid anchorage in applications such as retaining walls or slopes, those are still designed under the assumption of a linear, only combined load transfer from geogrid to soil without further differentiation along the geogrid anchorage length (EBGEO, 2011; BS 8006, 2010). Moreover, it is well-known that beside the surface friction a considerable part of the pull-out resistance is caused by the transverse elements of the geogrid structure (e.g. Palmeira, 2004).

As side effect of the recent implementation of new regulations for waste disposal sites in Germany and the herein required life time of 100 years, the need for an explicit calculation of geogrid forces and its deformation and displacement has arisen again. Therefore, in this paper, a one-dimensional interaction model is presented that incorporates a simple model for the description of the bearing resistance of transverse geogrid elements (Ziegler & Timmers, 2004) that has recently been verified by Müller (2011). The necessary input functions for the model are evaluated using tensile tests and pull-out tests with specially modified geogrid samples carried out at RWTH Aachen University, and the calibrated simulation results of regular pull-out tests in a normal-sized device are presented.

Additionally, the interaction model is validated with the results of large scale pull-out tests carried out at TU Clausthal, Germany. Finally, field measurements of a geogrid anchorage trench at the waste disposal site “Pochsandhalde”, Zellerfelder Tal, Germany are presented that are ideal for the validation of the model in an in-situ situation.

2 DEVELOPMENT OF NONLINEAR INTERFACE MODEL

2.1 *Interaction mechanisms and their modelling*

Many researchers have studied the interaction mechanisms of geogrids with soil using pull-out tests (Jewell et al., 1984; Lopes, 2002; Palmeira, 2004; Palmeira, 2009; Sieira et al., 2009) and all agree that there are two basic mechanisms:

- Friction, mainly on the longitudinal geogrid elements
- Bearing, a passive earth pressure developing in front of the transverse geogrid elements

Ziegler & Timmers (2004) put forward a simple model to describe this displacement-dependent bearing in front of the transverse elements as passive earth resistance against the movement of a geogrid element transverse to the soil (see Fig. 1). It is known that with increasing relative displacement between the two materials the mobilized area of this passive resistance also increases and the bearing resistance in front of one transverse element T_{xmd} is assumed to be the integrated shear stress τ_S on top and bottom of the mobilized soil area:

$$\begin{aligned} T_{xmd} &= 2 \cdot \int_A \tau_S \; dA \cdot n_g = 2 \cdot \int_A \sigma_N \cdot \tan \varphi_S \; dA \cdot n_g \\ &= 2 \cdot \sigma_N \cdot \tan \varphi_S \cdot a_L \cdot mob\, L\left(u_{xmd}\right) \cdot n_g \end{aligned} \qquad (1)$$

where A = mobilized area of passive earth resistance, n_g = number of longitudinal geogrid elements per unit width, σ_N = normal pressure in geogrid plane, φ_S = internal friction angle of the soil, a_L = aperture width between two longitudinal elements as in Fig. 1, and *mob L*(u_{xmd}) = mobilized length of passive earth resistance, depending on the transverse element displacement u_{xmd}

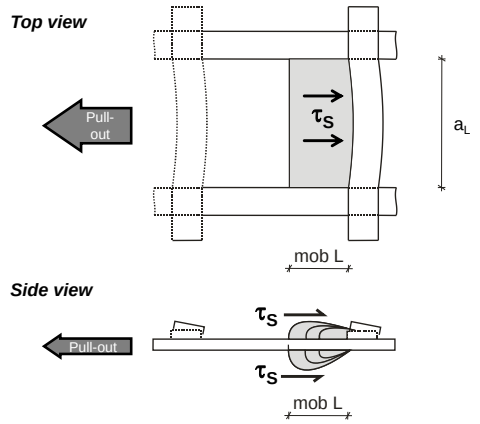

Figure 1. Model of bearing resistance in front of transverse geogrid elements.

Müller (2011) used and verified the above proposed model to simulate a fictional pull-out test, where the plane geogrid is modelled in one-dimension and is divided into a finite number of longitudinal segments. These segments are either pure frictional longitudinal segments or frictional longitudinal segments with a connected transverse element so that the mobilized earth pressure is transferred to the longitudinal segment at this point. The tensile load (per unit width) T_i and the displacement u_i at one end of each segment as in Figure 2 are calculated by:

$$T_i = T_{i-1} + 2 \cdot \Delta L \cdot W_1 \cdot \sigma_N \cdot \tan\left(\delta\left(u_{i-1}\right)\right) \cdot n_g + T_{xmd,i}\left(u_{i-1}\right) \qquad (2)$$

$$u_i = u_{i-1} + \varepsilon\left(T_i\right) \cdot \Delta L \qquad (3)$$

where ΔL = segment length, W_1 = width of longitudinal geogrid element, δ = friction angle between longitudinal element and soil, $T_{xmd,i}$ = bearing load in front of transverse element to be transferred to longitudinal element as in Eq. (1), and ε = strain of longitudinal geogrid element

The distributions along the geogrid of the tensile load and displacement can be calculated with Equations (2) and (3) in connection with Equation (1) when boundary conditions and functions for $\delta(u)$, *mob L*(u_{xmd}) and $\varepsilon(T)$ (see Fig. 2, right) are known. In the following chapter the experimental evaluations of those three functions are described.

2.2 *Evaluation of input functions*

2.2.1 *Load-strain behavior, tensile and junction strength of geogrid*

The load-dependent geogrid strain in longitudinal direction $\varepsilon(T)$ as well as the tensile load and strain at failure are obtained with tensile tests. Due to the viscosity of the polymers, geogrids creep under load. Therefore, when subjected to long-lasting loads, the material behavior is less stiff than obtained by short-term tensile tests and the load-strain curves obtained from creep tests have to be applied. The strength of the joints between longitudinal and transverse geogrid elements is obtained with tests according to GRI-GG2-87 (1987).

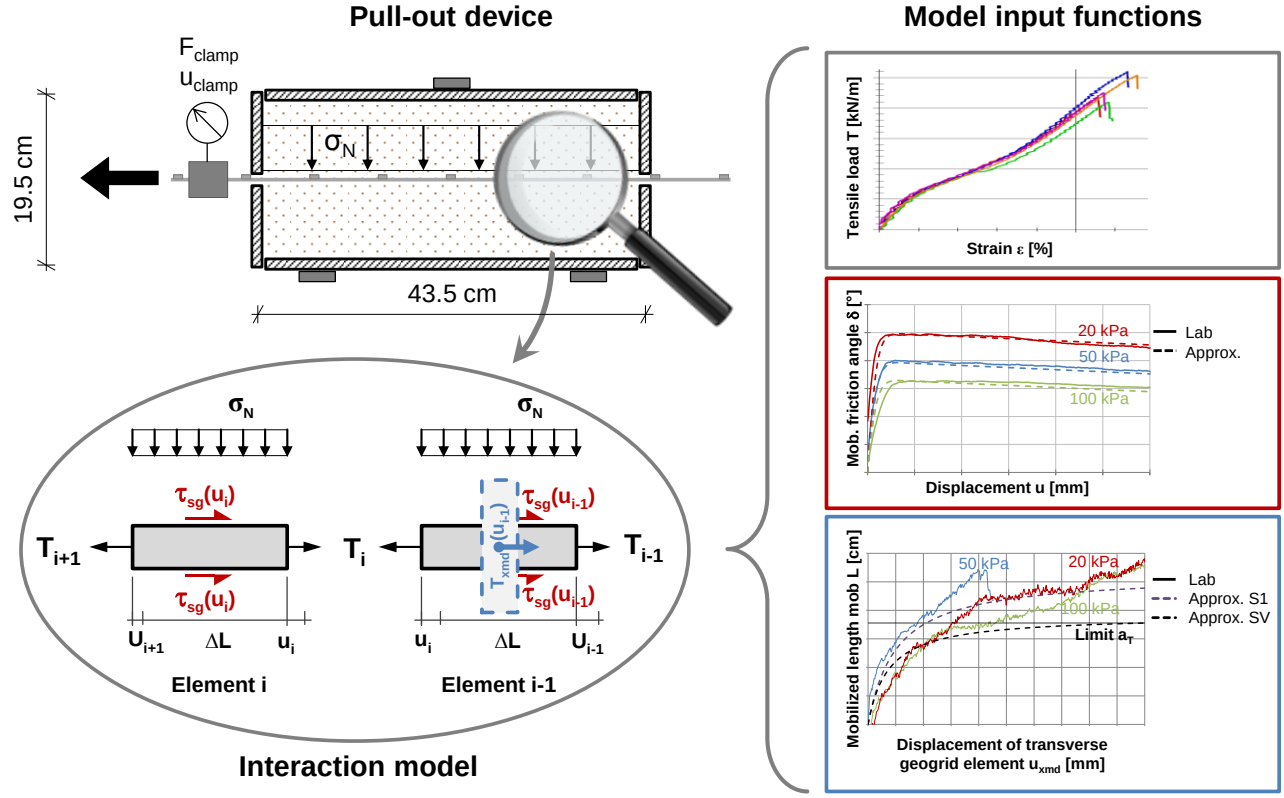

Figure 2. Pull-out test device, developed interaction model (left) and model input functions evaluated from tensile tests and special pull-out tests with modified geogrid specimens (right).

2.2.2 *Mobilized friction angle between longitudinal geogrid elements and soil*

The friction angle between the longitudinal geogrid elements and the soil is displacement-dependent and, especially with dilatant soils, also dependent on the normal pressure between the two materials. Therefore, it is obtained with pull-out tests of modified geogrid specimens consisting of only the longitudinal elements (so-called S0-tests). The mobilized friction angle in such test can be calculated from the measured tensile force at the clamp and the contact surface within the pull-out box, and it is approximated as a split function of the tangent hyperbolicus and a linear slope:

$$\delta(u) = \delta_{max}(\sigma_N) \cdot \frac{\tanh u}{c_{tanh}} \qquad \text{for } u \le u_g$$

$$\delta(u) = \delta_{max}(\sigma_N) \cdot \frac{\tanh u_g}{c_{tanh}} - m_\delta \cdot (u - u_g) \qquad \text{for } u \le u_g \qquad (4)$$

where $\delta_{max}(\sigma_N)$ = maximum friction angle dependent on the normal contact pressure σ_N, c_{tanh} = calibration factor depending on the geogrid tensile stiffness, m_δ = slope of decline of friction angle with increasing displacement after peak, u_g = relative displacement where peak friction angle is reached

The mobilized friction angle in the tests, evaluated using the measured clamp force, disregards the varying displacements along the contact surface so that the model input function as in Equation (4) has to be calibrated with c_{tanh} depending on the geogrid tensile stiffness.

2.2.3 *Mobilized bearing resistance in front of transverse geogrid elements*

According to the model, developed by Ziegler & Timmers (2004) and shown in Figure 1, the bearing resistance in front of a transverse geogrid element, which is transferred into the longitudinal element via the junctions, develops with the mobilized length *mob L* of the passive earth pressure.

In the laboratory, the bearing resistance of one transverse element can be evaluated by comparing the measured clamp resistance against pull-out T_{clamp} of a specimen with one transverse element (S1) and a specimen without any transverse elements (S0):

$$T_{xmd}\left(u_{xmd}\right) = T_{clamp}^{S1}\left(u_{xmd}\right) - T_{clamp}^{S0}\left(u_{xmd}\right) \tag{5}$$

Equalizing and rearranging Equations (1) and (5) gives the mobilized length from the laboratory test:

$$mob\ L\left(u_{xmd}\right) = \frac{T_{clamp}^{S1}\left(u_{xmd}\right) - T_{clamp}^{S0}\left(u_{xmd}\right)}{2 \cdot \sigma_N \cdot \tan\varphi_S \cdot a_L \cdot n_g} \tag{6}$$

The obtained curves of one geogrid-soil combination for various normal pressures approximately coincide so that the experimental curves can be approximated by one hyperbolic function for all normal pressures:

$$mob\ L\left(u_{xmd}\right) = \frac{u_{xmd}}{a_{S1} + b_{S1} \cdot u_{xmd}} \tag{7}$$

where a_{S1}, b_{S1} = hyperbolic parameters for mobilized length of S1-test with one transverse element

Obviously, in a regular geogrid with all transverse elements (SV) the mobilized length cannot increase indefinitely as it reaches the next transverse element in front. Therefore, the mobilized length is limited by the aperture between two transverse elements a_T (see input function of mobilized length in the right bottom part of Fig. 2):

$$mob\ L\left(u_{xmd}\right) = \frac{u_{xmd}}{a_{SV} + b_{SV} \cdot u_{xmd}} \le a_T \tag{8}$$

All three input functions that are described in this chapters are shown in the right part of Figure 2.

2.3 *Calibration with pull-out tests*

The input functions of the mobilized friction angle between longitudinal geogrid element and soil and the mobilized length of the developing earth pressure resistance in front of transverse elements have been evaluated from pull-out tests with specifically modified geogrid samples, as described in the previous chapters. Figure 3 shows the test and simulation results of those specific tests (S0 – without transverse elements; S1 – with one transverse element; SV – with a regular geogrid). The soil was gravel with the maximum particle size of 32 mm and a normal pressure of $\sigma_N = 20\ kPa$ was applied. The characteristic result of a pull-out test is shown by the measured force at the clamp F_{clamp}, i.e. the pull-out resistance, over the displacement at the clamp u_{clamp}. With the justified calibration of few parameters of the input functions, Figure 3 shows that the developed interaction model is capable of reproducing the test results accurately. Only the simulation curve of the S1-test varies to the laboratory result, as one bearing mobilization function has been calibrated for various tests with different normal pressures so that for those S1-tests only on average a good calibration has been reached. The results of those S1-tests have varied because the arbitrary particle location can influence the total pull-out resistance considerably as only one transverse geogrid element was involved.

With the model and the corresponding simulation tool it is possible to calculate the tensile force, strain and displacement distributions along the anchorage length of the geogrid. Exemplarily, in Figure 4, the force distributions are drawn for the three tests (S0, S1 and SV) from Figure 3 and for a clamp displacement of $u_{clamp} = 30\ mm$. Both discussed interaction mechanisms are visible; frictional load transfer occurs along the geogrid at all positions so that the tensile load decreases within the pull-out box almost linearly. At each transverse geogrid element the bearing resistance in front of it is mobilized and is transferred to the longitudinal element via its junctions, visible in Figure 4 as a jump in the force distribution line.

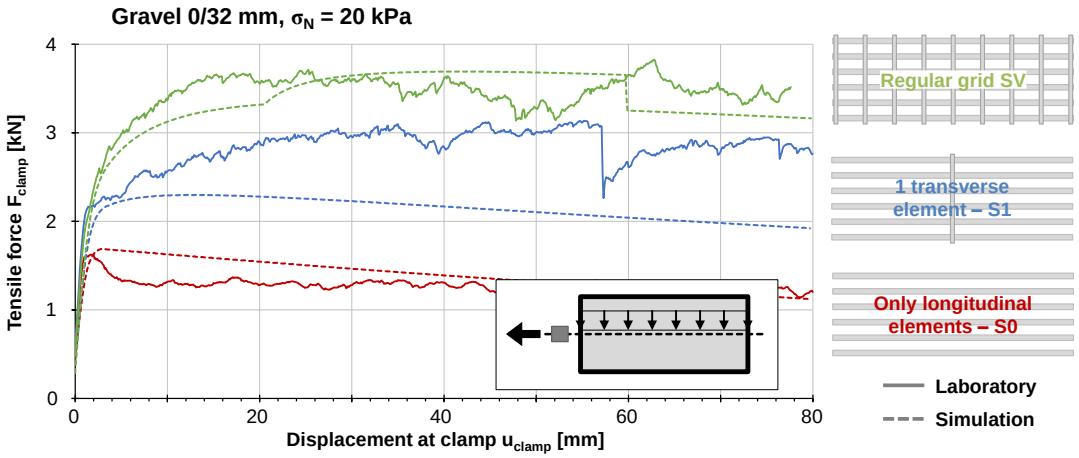

Figure 3. Pull-out test and simulation results for tests in gravel with a normal pressure of σ_N = 20 kPa with modified geogrids (no transverse elements – S0, one transverse element – S1) and a test with a regular geogrid (SV).

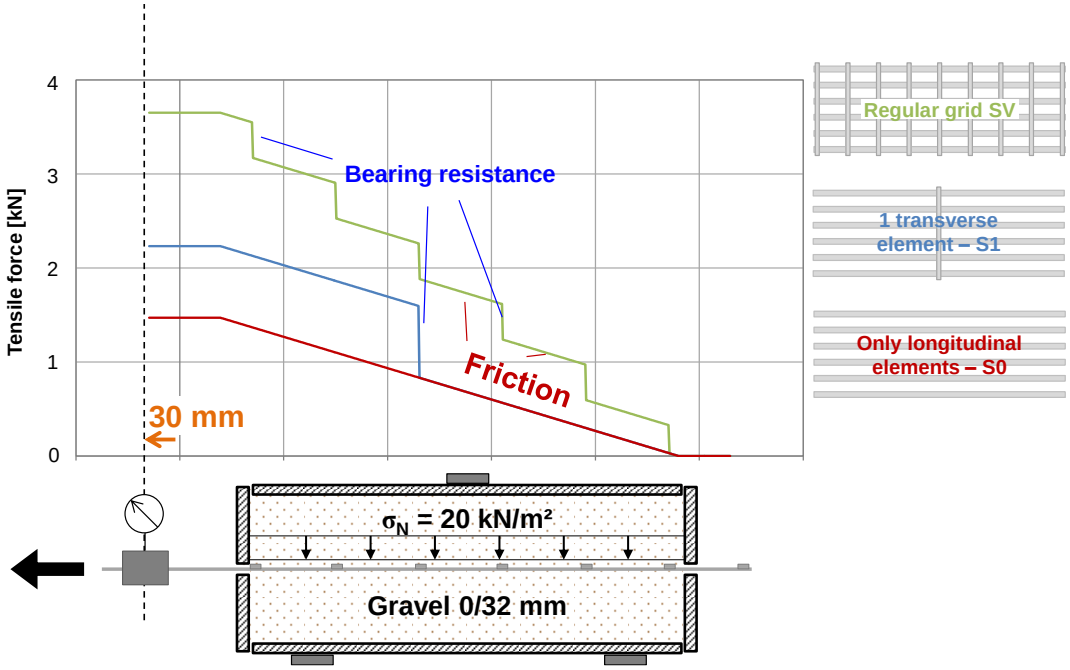

Figure 4. Modeled tensile force distributions along the geogrid for tests in gravel with a normal pressure of σ_N = 20 *kPa* with modified geogrids (no transverse elements – S0, one transverse element – S1) and a test with a regular geogrid (SV).

The influence of the transverse elements on the pull-out resistance of geogrids is shown clearly in Figures 3 and 4 as the overall pull-out resistance has been increased considerably. The mobilized bearing resistance of those transverse elements develops with increasing relative displacement and the frictional load transfer decreases the tensile load within the geogrid between the transverse elements. Therefore, the load on each junction that has to be transferred decreases along the anchorage length (from left to right in Fig. 4, hardly visible due to the high tensile stiffness of the geogrid).

3 VALIDATION OF MODEL WITH LARGE PULL-OUT TESTS

For the validation of the developed interaction model, pull-out tests carried out in a large pull-out device at the Institute of Geotechnical Engineering and Mine Surveying, TU Clausthal, Germany have been simulated (Prüfbericht TU Clausthal, 2012). The pull-out box had dimensions of 150 x 60 x 60 cm^3 (L x W x H), the geogrid anchorage length was 120 *cm* and, in the presented tests, the same soil (gravel 0/32 *mm*) and same geogrid type were used as in the tests with the small pull-out box described above. Figure 5 shows the resulting pull-out resistance of various tests (with regular geogrids) at three different normal pressures σ_N. Due to uncertain boundary conditions in the area of the geogrid clamp, the pull-out force at the clamp F_{clamp} in Figure 5 is not drawn over the displacement of the clamp u_{clamp} but the geogrid displacement at the front of the pull-out box u_{DT}, measured by a displacement transducer. According to

each normal pressure, a simulation has been carried out and the resulting pull-out resistance is also shown in Figure 5.

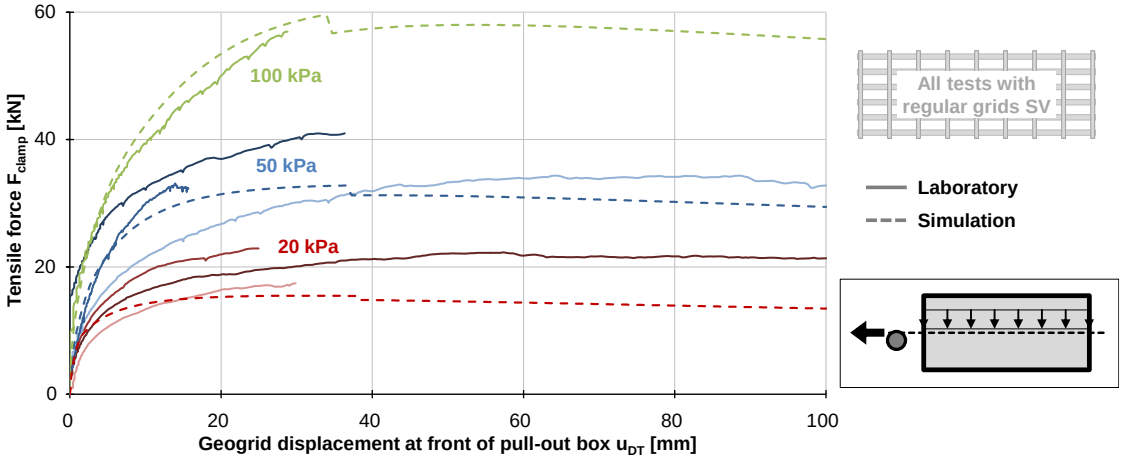

Figure 5. Results of pull-out tests with regular geogrids in a large pull-out device with various normal pressures (Institute of Geotechnical Engineering and Mine Surveying, TU Clausthal) and their simulations.

It is important to note that the model input functions, obtained by calibration with the small pull-out tests described in chapter 2, have been used for the simulation of the large pull-out tests without any modification. In spite of the considerable deviation between the laboratory tests with the same normal pressure, it can be seen that the development of the pull-out resistances and their maximums have been reproduced well with the developed interaction model, only the simulation of the tests at 20 *kPa* underestimates the measured pull-out resistance slightly.

To further compare the test and simulation results, the geogrid displacement and strain distributions are drawn in Figure 6 along the geogrid anchorage length for three pull-out states. Displacements and strains were measured during the tests with several displacement transducers and strain gauges connected to the geogrids. The measured displacement and strain distributions are both reproduced very well with the interaction model, except for the very high displacements measured at the clamp, caused by unintended slip between geogrid and clamp in the laboratory tests.

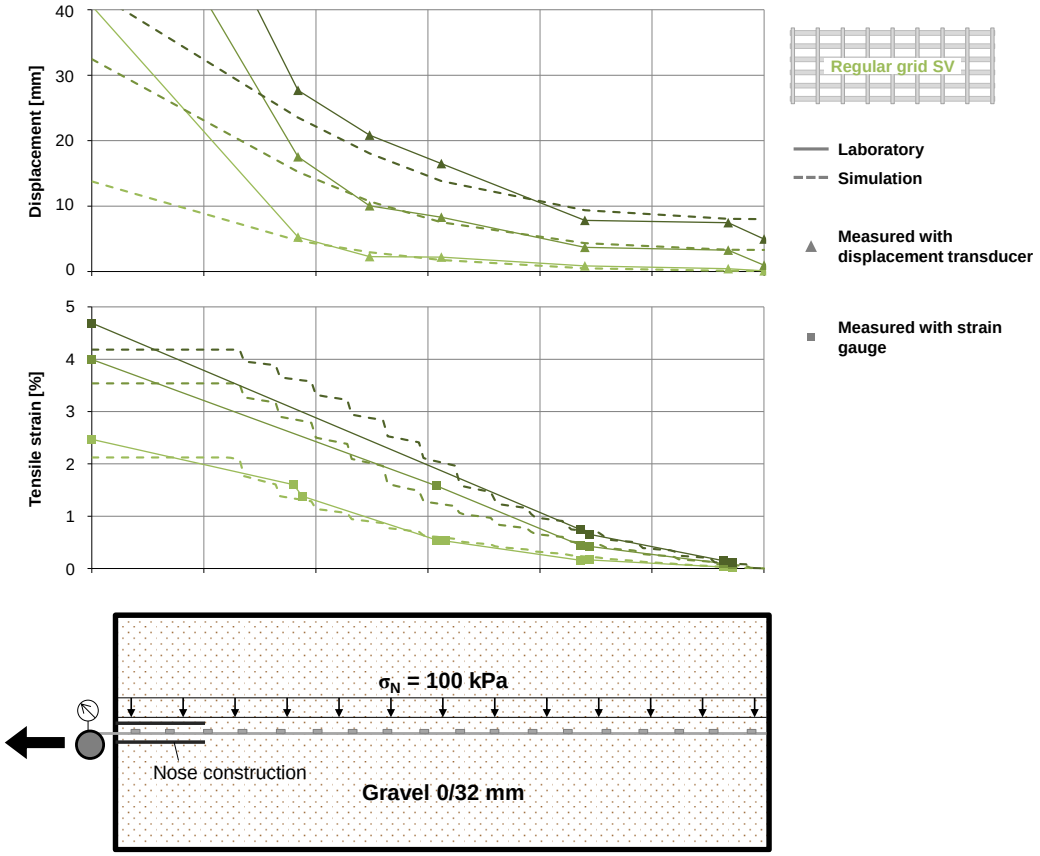

Figure 6. Measured and modeled displacement and strain distributions along the geogrid of three pull-out states for a test with a regular geogrid in gravel with the normal pressure of σ_N = 100 *kPa*.

4 FIELD INVESTIGATION OF GEOGRID ANCHORAGE TRENCH

At the waste disposal "Pochsandhalde", Zellerfelder Tal in Germany a new surface sealing was installed in 2010. To reach an efficient ratio of *deposited waste* to *land use* a steep slope was built that had to be secured with geogrids against failure by sliding down. In such a geogrid reinforced slope, the downward-directed forces are held back by the geogrids and accumulate from bottom to top along the geogrids. At the top of the slope these tensile forces have to be anchored, i.e. transferred to the surrounding soil in an anchorage trench, shown in Figure 7. In such an anchorage trench a classic pull-out situation occurs; high tensile forces in the geogrids have to be transferred to the surrounding soil along a short anchorage length, demanding high shear stresses. In contrast to pull-out situations in other geogrid reinforced structures, the failure mode "pull-out" is actually decisive for design in anchorage trenches due to the low overburden.

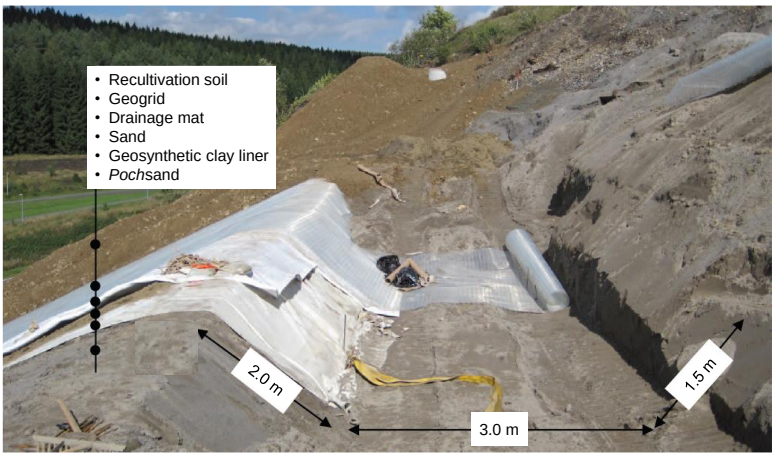

Figure 7. Construction of geogrid anchorage trench of surface slope at the disposal Pochsandhalde in Germany, instrumented with strain gauges (after Haaszio et al., 2011).

To investigate the interaction and load transfer behavior between geogrid and soil in situ, the geogrid at the disposal Pochsandhalde was instrumented within the anchorage trench. In Figure 8, the geogrid strains, measured with strain gauges, along the anchorage length are shown for three different monitoring states. The first two states represent the construction of the slope when the geogrid was gradually loaded and the third strain distribution occurred after the construction was terminated (1080 *min*), i.e. the geogrid was fully loaded (Vollmert et al., 2012).

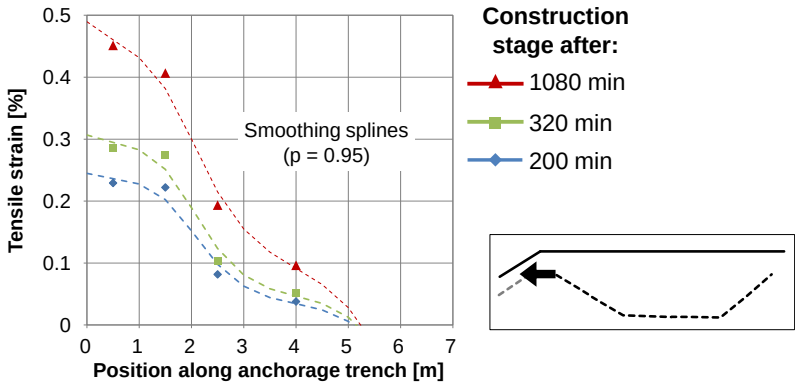

Figure 8. Measured geogrid strains within the anchorage trench of the disposal Pochsandhalde and fitted smoothing splines for three monitoring states.

As in many geogrid reinforced structures, the measured geogrid strains are small and do not reach 0.5 % for the highest loading state. However, the strain gauge at 4 *m* within the anchorage trench already reported for the first monitoring state a considerable tensile strain, showing that the geogrid has been activated along almost its complete anchorage length already at low tensile loads. Furthermore, the shape of the strain distribution curves is clearly not linear, which indicates that an advanced interface model is necessary to be able to calculate the complex pull-out behavior of geogrids.

5 SUMMARY AND CONCLUSION

A one-dimensional model has been presented to describe the pull-out behavior of geogrids embedded in soil. It takes into account both interaction mechanisms, i.e. friction on the geogrid surfaces and bearing as passive earth pressure in front of the transverse geogrid elements. For the model, three necessary input functions were identified; first, the load-strain behavior including tensile strength was obtained with short-term tensile tests or creep tests when modelling long-term loads. Second, the displacement-dependent mobilized friction angle between longitudinal geogrid element and soil was measured using pull-out tests of geogrid samples without any transverse elements. Third, the mobilized length of the developing zone of passive earth bearing resistance in front of a transverse geogrid element was found for a single transverse element and further evaluated for the situation along a regular geogrid with many transverse elements. With a reasonable calibration of few parameters of the input functions, the model yielded good results in comparison to regular pull-out tests conducted at RWTH Aachen University.

For validation, the developed interaction model was applied to simulate large pull-out tests carried out at TU Clausthal, Germany and the modeled results were in good agreement with the experimental results. At last, field measurement data of an instrumented geogrid in an anchorage trench at the top of a surface sealing slope at the waste disposal site Pochsandhalde in Germany was presented. During construction, and thereby, gradual tensioning of the geogrid, it was observed that already for small loads the geogrid within the anchorage trench was activated almost along its complete anchorage length. After completion of construction the maximum geogrid tensile strain was approximately 0.45 %.

With the developed model, for a given action, e.g. design load, it is possible to calculate the respective deformation and displacement of the geogrid as well as the geogrid force and junction loads at all positions along its anchorage length. As next step, the model will be validated using the presented field data so that for in-situ applications serviceability and ultimate limit states can be predicted and existing factors of safety can be calculated.

REFERENCES

British Standard, B.S. 8006-1 2010. Code of practice for strengthened/reinforced soils and other fills.

Deutsche Gesellschaft für Geotechnik (DGGT) 2011. Recommendations for Design and Analysis of Earth Structures using Geosynthetic Reinforcements – EBGEO. John Wiley & Sons, 2011.

GRI-GG2-87 1987. Geogrid junction strength. Geosynthetic Research Institute, Philadelphia, USA.

Haaszio, S., Werth, K. & Tebbe, J. 2011. Sanierung Pochsandhalde Zellerfelder Tal, Planung und Ausführung eines 1:2 geneigten Oberflächenabdichtungssystems unter Einsatz von hochzugfesten Geogittern. 7. Leipziger Deponiefachtagung „Stilllegung, Sicherung, Nachsorge und Nachnutzung von Deponien“, Leipzig, Germany.

Jewell, R.A., Milligan, G.W.E., Sarsby, R.W. & Dubois, D. 1984. Interaction between soil and geogrids. Proc. Symp. on Polymer Grid Reinforcement in Civil Engineering, p. 18-30. Science and Engineering Research Council and Netlon Ltd..

Lopes, M.L. 2002. Soil-geosynthetic interaction. Geosynthetics and their applications, Ed. Shukla, S. K.., Thomas Telford.

Müller, W. 2011. Zur Bemessung der Verankerung von Bewehrungsgittern aus Kunststoff beim Schutz von Böschungen vor hangparallelem Gleiten, (in German). Bautechnik, 88.6, p. 347-361.

Palmeira, E.M. 2004. Bearing force mobilisation in pull-out tests on geogrids. Geotextiles and Geomembranes, 22: p. 481-509.

Palmeira, E.M. 2009. Soil-geosynthetic interaction: Modelling and analysis. Geotextiles and Geomembranes, 27, p. 368-390.

Prüfbericht TU Clausthal 2012. Untersuchung des Kraftverlaufes über die Einbindelänge bei Pull-Out Versuchen an Secugrid 200/40 R6 2012-04-13 (unpublished).

Sieira, A C C.F., Gerscovich, D.M.S., Sayão, A.S.F.J. 2009. Displacement and load transfer mechanisms of geogrids under pullout condition. Geotextiles and Geomembranes, 27: p. 241-253.

Vollmert, L., Werth, K., Emersleben, A. & Holm, B. 2012. In-Situ-Beanspruchungen eines Geogitters im Verankerungsbereich einer Oberflächenabdichtung am Beispiel der Pochsandhalde Zellerfelder Tal. 28. Fachtagung „Die sichere Deponie - Sicherung von Deponien und Altlasten mit Kunststoffen“, Würzburg, Germany.

Ziegler, M. & Timmers, V. 2004. A new approach to design geogrid reinforcement. Proc. 3rd Europ. Geosynthetics Conf., Munich, Germany, p. 661-667.